Expectation for Neutrino-Argon interactions in the Short-Baseline Near Detector (SBND)

Author:
Giacomo SCANAVINI
University of Pisa, Italy

Supervisor:
Dr. Ornella PALAMARA

August-September, 2015

Contents

1 Introduction

This report explains my work at Fermilab during the summer project in the period between August and September in 2015. I worked with the SBND collaboration on expectations for neutrino-argon interactions. I was given a simulation made with GENIE (v2.8) in the Short-Baseline Near detector (SBND) active volume (112 tons) for a period run of 3 years ($6.6 \cdot 10^{20}$ proton on target (POT)) and I analysed charged-current 0π and 1π final state channels and rare channels such as neutrino elastic scattering. The introduction gives first an overview on MiniBooNE results and low energy anomaly (1.1), and in later a description of liquid argon TPC (LAr-TPC) technology used in SBND and in the other two detectors of the Short-Baseline Neutrino(SBN) project (1.2).

1.1 MiniBooNE Results and Low Energy Anomaly

The MiniBooNE experiment at Fermilab measured neutrino interactions 540 meters from the target of the Booster Neutrino Beam (BNB).
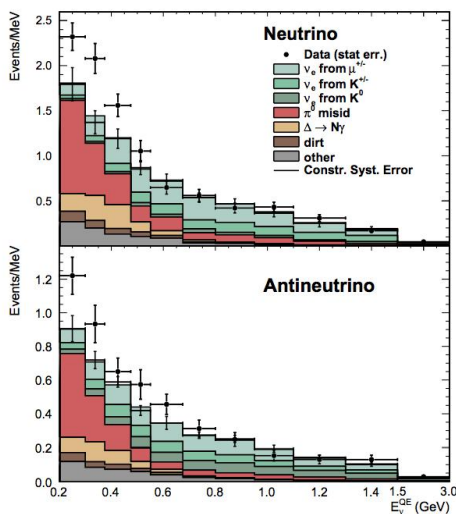
Figure 1: $\overline{\nu}_e$ (top) and ν_e (bottom) candidate events and predicted backgrounds showing the observed excesses in the MiniBooNE data.

Muon and electron neutrinos are identified in charged-current (CC) interactions by the characteristic signatures of Cherenkov rings for muons and electrons. In a ten year data set including both neutrino and anti-neutrino running [8-10], MiniBooNE has observed a 3.4σ signal excess of ν_e candidates in neutrino mode (162.0 ± 47.8 electromagnetic events) and a 2.8σ excess of $\overline{\nu}_e$ candidates in anti-neutrino mode (78.4 ± 28.5 electromagnetic events) as shown in figure 1. The excess events can be evenly associated to electrons or single photons since these are indistinguishable in MiniBooNEs Cherenkov imaging detector. MicroBooNE will address this

question at the same baseline as Mini-BooNE by utilizing the added capability to separately identify electrons and photons. The most common interpretation of this collection of data is evidence for the existence of one or more additional, mostly sterile neutrino states with masses at or below the few eV range. The minimal model consists of a hierarchical 3+1 neutrino mixing, acting as a perturbation of the standard three-neutrino model dominated by the three ν_e , ν_μ and ν_τ active neutrinos with only small contributions from sterile flavours. The new sterile neutrino would mainly be composed of a heavy neutrino ν_4 with mass m_4 such that the new $\Delta m^2 = \Delta m^2_{41}$ and m_1, m_2, $m_3 << m_4$ with $\Delta m^2_{41} \simeq [0.1 \quad 10]$ eV^2.

1.2 LAr-TPC Technology

Looking for the low energy excess observed by the MiniBooNE experiment [8] and characterizing its nature is the main physics goal of the MicroBooNE experiment [11]. This excess of electromagnetic events could be due to neutrino interactions with either a single-electron or single-photon in the final state. With the introduction of the LAr-TPC technology a full 3D imaging, precise calorimetric energy reconstruction and efficient particle identification allow for exclusive topology recognition based on final state particle multiplicity. In the TPC electrons and gammas have different charge yields, gamma will pair produce and the resulting lower-energy electron and positron have different ionization energy loss in their first few centimeters of track than a single electron with an energy twice bigger. Shower containment is not fully needed in order to discriminate an electron from a single photon. For this reason both SBND and MicroBooNE will be able to investigate on the low energy electron-like excess at different distances from the target of the BNB. Besides, with this type of detector it is possible to measure kinematic distribution for most of the particles in the final state.
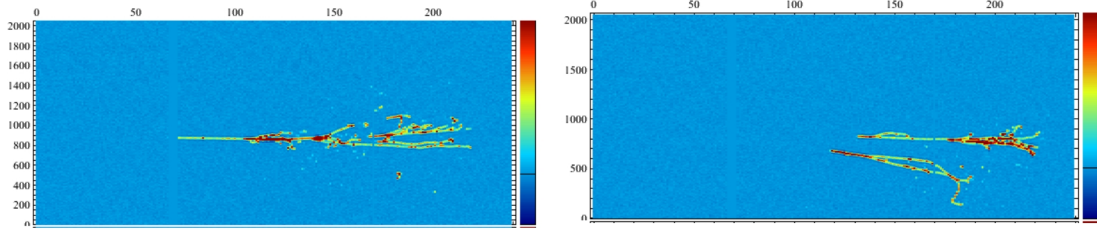
Figure 2: Left: electron electromagnetic shower reconstructed in liquid argon. Right: π^0 decay into two γ. The initial part of each shower has a different ionization energy loss, in this way particles get recognizable.
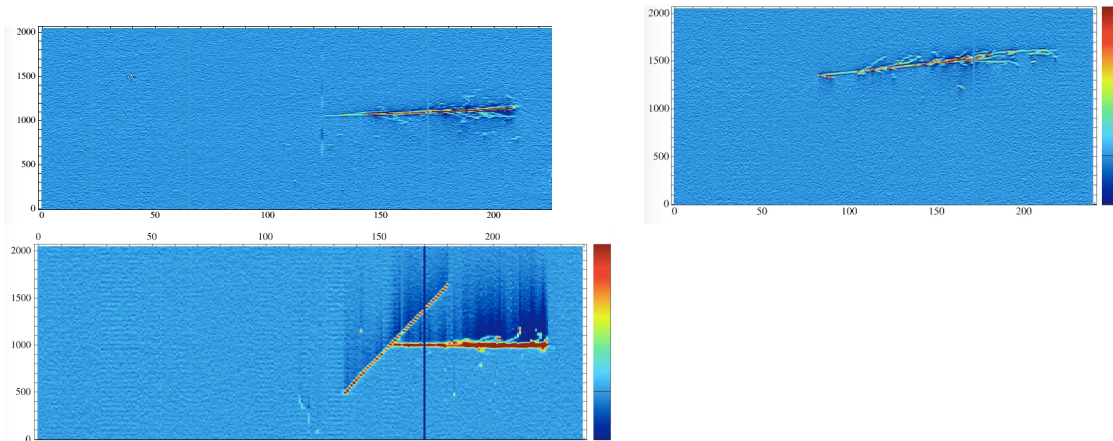
Figure 3: Clockwise: 0 proton, 1 proton and 2 protons reconstructed at the main vertex for these three CC ν_e events in liquid argon.

4

2 Short-Baseline Neutrino (SBN) Project

The future short-baseline experimental configuration is proposed to include three Liquid Argon Time Projection Chamber detectors (LAr-TPCs) located on-axis in the BNB at Fermilab. All three detectors that take part to SBN project are summarized in figure 4.

Detector	Distance from BNB Target	LAr Total Mass	LAr Active Mass
LAr1-ND	110 m	220 t	112 t
MicroBooNE	470 m	170 t	89 t
ICARUS-T600	600 m	760 t	476 t

Figure 4: Summary of the SBN detector locations and masses.

The detector locations were chosen to optimize sensitivity to neutrino oscillations and minimize the impact of flux systematic uncertainties as reported in [1]. Figure 5 shows the locations of the detectors superimposed on an aerial view of the Fermilab neutrino experimental area.

This section gives a BNB description (2.1) and a briefly introduction on the detectors of the SBN project (2.2, 2.3 and 2.4) including the SBND detector which is the one the simulation I used for the report is based on.

2.1 Booster Neutrino Beam (BNB)

The Booster Neutrino Beam is created by extracting protons from the Booster accelerator at 8 GeV kinetic energy (8.89 GeV/c momentum) and impacting them on a beryllium (Be) target to produce a secondary beam of hadrons, mainly pions. Charged secondaries are focused by a single toroidal aluminum alloy focusing horn that surrounds the target. The horn can be pulsed with either polarity, thus focusing either positives or negatives and de-focusing the other. Focused mesons are allowed to propagate down a 50 m long, 0.91 m radius air-filled tunnel where the majority will decay to produce muon and electron neutrinos. The remainder are absorbed into a concrete and steel absorber at the end of the 50 m decay region. Suspended above the decay region at 25 m are concrete and steel plates which can be deployed to reduce the available decay length, thus systematically altering the

Figure 5: Map of the Fermilab neutrino beamline area showing the axis of the BNB (yellow dashed line) and approximate locations of the SBN detectors at 110 m, 470 m, and 600 m. The pink line indicates the axis of the NuMI neutrino beam for reference.

neutrino fluxes. A schematic of the BNB target station and decay region is shown in figure 6.

Systematic uncertainties associated with the beam have also been characterized in a detailed way as seen in [2-3] with a total error of $\sim$9% at the peak of the ν_μ flux and larger in the low and high energy regions. The neutrino fluxes observed at the three SBN detector locations are shown in figure 7. Note the rate in the SBND is 20-30 times higher than at the MicroBooNE and ICARUS locations.

The composition of the flux in neutrino mode (focusing positive hadrons) is energy dependent, but is dominated by ν_μ ($\sim$93.6%), followed by $\overline{\nu}_\mu$ ($\sim$5.9%), with an intrinsic $\nu_e/\overline{\nu}_e$ contamination at the level of $\sim$0.5% at energies below 1.5 GeV.
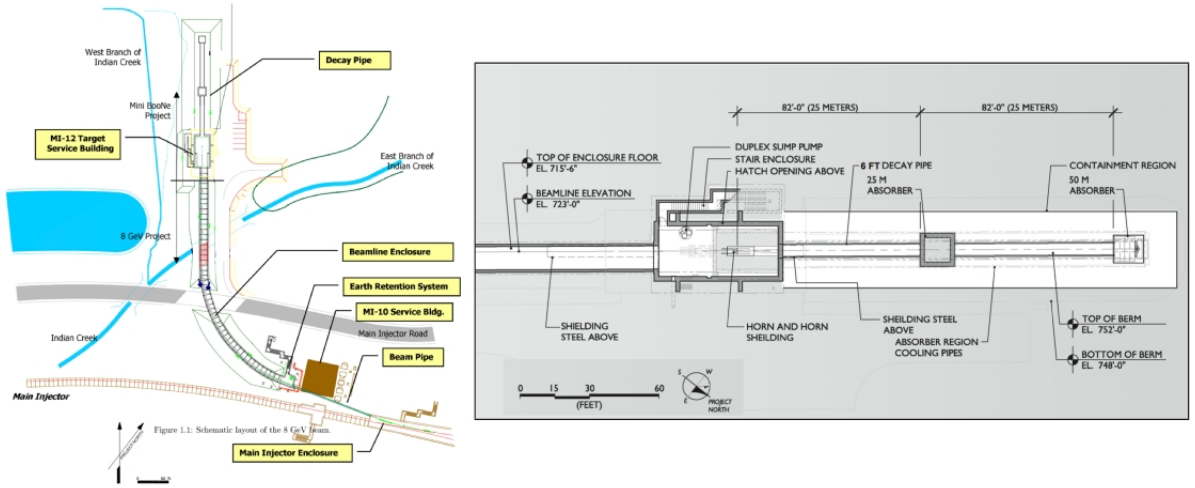
Figure 6: Schematic drawings of the Booster Neutrino Beamline including the 8 GeV extraction line, target hall and decay region.
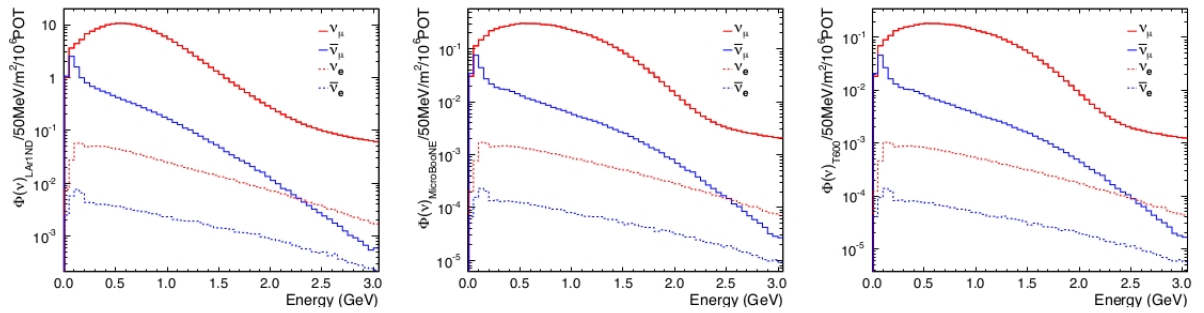
Figure 7: The Booster Neutrino Beam flux at the three SBN detectors: (left) SBND, (center) MicroBooNE, and (right) ICARUS-T600.

2.2   MicroBooNE

The experiment measures neutrino interactions in argon for multiple reaction channels and investigate the source of the currently unexplained excess of low energy electromagnetic events observed by MiniBooNE. The MicroBooNE detector is a 170 ton total mass (89 ton active mass) liquid argon TPC contained within a conventional cryostat [4]. The active region of the TPC is a rectangular volume of dimensions 2.33 m x 2.56 m x 10.37 m. The MicroBooNE TPC design allows ionization electrons from charged particle tracks in the active liquid argon volume to drift up to 2.56 meters to a three-plane wire chamber. An array of 32 PMTs are mounted behind the wire planes on the beam right side of the detector to collect prompt scintillation light produced in the argon [5]. MicroBooNE is approved to receive an exposure of $6.6 \cdot 10^{20}$ POT in neutrino running mode from the BNB. It also records interactions from an off-axis component of the NuMI neutrino beam. During MicroBooNE running, the BNB will be operated in the same configuration that successfully delivered neutrino and anti-neutrino beam to Mini-BooNE, thereby significantly reducing systematic uncertainties in the comparison of MicroBooNE data with that from MiniBooNE.

2.3   ICARUS-T600

The ICARUS-T600 detector previously installed in the underground INFN-LNGS Gran Sasso Laboratory has been the first large-mass LAr-TPC operating as a continuously sensitive general purpose observatory. The successful operation of the ICARUS-T600 LAr-TPC demonstrates the enormous potential of this detection technique, addressing a wide physics program with the simultaneous exposure to the CNGS neutrino beam and cosmic-rays [6]. The ICARUS-T600 detector consists of two large identical modules with internal dimensions 3.6 x 3.9 x 19.6 m^3 filled with ∼760 tons of ultra-pure liquid argon, surrounded by a common thermal insulation [6-7]. Each TPC is made of three parallel wire planes. A uniform electric field of 500 V/cm is applied to the drift volume. A three-dimensional image of the ionizing event is reconstructed combining the wire coordinate on each plane at a given drift time with ∼1 mm^3 resolution over the whole active volume (340 m^3 corresponding to 476 tons). The ICARUS-T600 detector has been moved to CERN for an overhauling preserving most of the existing operational equipment,

while upgrading some components with up-to-date technology in view of its future near surface operation. The detector is expected to be transported to Fermilab at the beginning of 2017.

2.4   Short-Baseline Near Detector (SBND)

The basic concept is to construct a membrane-style cryostat in a new on-axis enclosure adjacent to and directly downstream of the existing SciBooNE hall. The membrane cryostat will house a CPA (Cathode Plane Assembly) and four APAs (Anode Plane Assemblies) to read out ionization electron signals. The active TPC volume is 4.0 m x 4.0 m x 5.0 m, containing 112 tons of liquid argon. Figure 8 shows the state of the conceptual design for the Near Detector building and the SBND TPC.
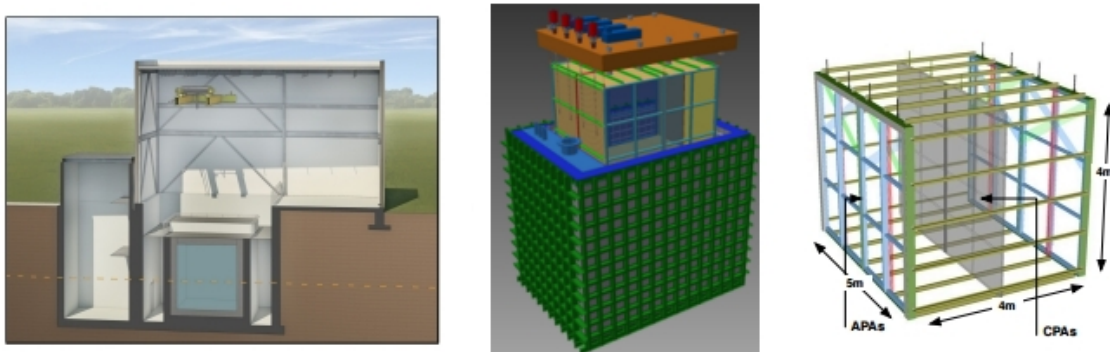
Figure 8: Left: The SBND detector building concept. The neutrino beam center is indicated by the orange dashed line and enters from the left. Right: The SBND TPC conceptual design.

The two APAs will each hold 3 planes of wires. The CPA has the same dimensions as the APAs and is centered between them. The drift distance between each APA and the CPA is 2 m such that the cathode plane will need to be biased at -100 kV for a nominal 500 V/cm field. The SBND design will additionally include a light collection system for detecting scintillation light produced in the argon volume.

3 Physics of SBND

While SBND, in conjunction with MicroBooNE and the ICARUS-T600, is a critical part of the neutrino oscillation physics, as a stand alone detector it enables a large number of relevant physics results. This section we will discuss a sub-set of the physics measurements that can be performed with SBND. These include studies of a possible MiniBooNE-like low energy excess of electromagnetic events that does not depend on the distance.

3.1 Electromagnetic Excess Distance Dipendence

Observation of a low energy excess signal by MicroBooNE in the years leading up to the beginning of SBND data taking would immediately lead to the question of whether that excess is intrinsic to the beam or appears over the 470 m distance between source and detector. SBND, at 110 m from the BNB target, can search for the same excess in a relatively short time. The event rate with which SBND will be able to study these events will be more than one order of magnitude larger than MicroBooNE. Such a sample will enable a measurement of this reaction with great precision and inform the development of cross section models in this energy range to include this process.

3.2 Neutrino Cross Section Measurement

Neutrino-nucleus interactions are critical to understand in neutrino oscillation experiments, including the future liquid argon long-baseline program. SBND provides an ideal venue to conduct precision cross section measurements in the GeV energy range. The experiment will collect enormous neutrino event samples, expectation are shown in figure 9, and, continuing the studies done by MicroBooNE and ICARUS, will make the worlds highest statistics cross section measurements for many ν-Ar scattering processes. A novel approach based on the event categorization in terms of exclusive topologies can be used to analyse data and provide precise cross section measurements in many different ν_μ and ν_e exclusive channels. It's also shown the classification by physical process from Monte Carlo truth information. The largest event sample corresponds to a ν_μ charged-current 0 pion final state, where there is an outgoing μ^-, one or more recoil nucleons, and no outgoing

pions or kaons. This cross section for scattering off nuclei largely depends on final state interactions and other nuclear effects and SBND data will allow the study of nuclear effects in neutrino interactions in argon nuclei with high precision. In SBND more than 2 million neutrino interactions will be collected per year in the full active volume (assuming $2.2 \cdot 10^{20}$ POT), with 1.5 million ν_μ and 12,000 ν_e charged-current (CC) events.

Comparison of ν_μ CC and ν_e CC cross sections is very important. By lepton universality, the cross sections should be the same after correcting for the outgoing charged-lepton mass. A difference in the cross sections would indicate a new process that violates lepton universality. SBND will also see several hundred ν_μ e $\rightarrow$ ν_μ e elastic scattering events in 6.6x10^{20} POT. These events are easily identified by an outgoing electron along the neutrino beam direction with cos$\theta > 0.99$ and with no recoil nucleons. With this event sample, a measurement of sin$^2\theta_W$ can be made at relatively low energy to be compared with the world average. Finally, a quarter million neutral-current (NC) elastic scattering events are expected, identified by a single nucleon (proton or neutron) recoil track.

CC 0 π ν_μ events		
Process	**N. events**	**Stat. uncert. (%)**
INCLUSIVE	3,503,955	0.05
QE	3,064,670	0.06
RES	357,035	0.17
DIS	79,847	0.35
0p	765,347	0.11
1p	2,014,640	0.07
2p	356,401	0.17
3p	163,532	0.25
4p	89,408	0.33
$\geq$5p	114,627	0.30

CC 0 π ν_e events		
Process	**N. events**	**Stat. uncert. (%)**
INCLUSIVE	22,279	0.67
QE	18,551	0.73
RES	2,694	1.93
DIS	964	3.22
0p	4,535	1.48
1p	12,177	0.91
2p	2,307	2.08
3p	1,268	2.81
4p	759	3.63
$\geq$5p	1,234	2.85

CC 1 π ν_μ events				CC 1 π ν_e events		
Process	**N. events**	**Stat. uncert. (%)**		**Process**	**N. events**	**Stat. uncert. (%)**
INCLUSIVE	1,056,440	0.10		INCLUSIVE	9,775	1.01
QE	18,785	0.73		QE	164	7.81
RES	809,550	0.11		RES	6,866	1.21
DIS	218,570	0.21		DIS	2,584	1.97
0p	279,525	0.19		0p	2,667	1.94
1p	537,112	0.14		1p	4,667	1.46
2p	155,347	0.25		2p	1,316	2.76
3p	41,585	0.49		3p	505	4.45
4p	19,985	0.71		4p	282	5.95
$\geq$5p	22,878	0.66		$\geq$5p	338	5.44
Pion type	**N. events**	**Stat. uncert. (%)**		**Pion type**	**N. events**	**Stat. uncert. (%)**
π^+	1,036,750	0.10		π^+	9,506	1.03
π^-	19,691	0.71		π^-	269	6.10

Figure 9: Estimated event rates for charged-current 0 π and 1 π final state channels using GENIE (v2.8) in the SBND active volume (112 ton) for a $6.6 \cdot 10^{20}$ POT exposure. In enumerating proton multiplicity, we assume an energy threshold on proton kinetic energy of 21 MeV. The 0 π and 1 π topologies include any number of neutrons in the event.

4   Expectation for SBND

In this section are reported some results of the analysis of the simulation made with GENIE (v2.8) for $6.6 \cdot 10^{20}$ POT. A selective process for neutrino elastic scattering events is reported in (4.1) while charged-current events with 0 π and 1 π are reported in (4.2).

4.1   Neutrino Elastic Scattering Event Selection

In neutrino experiments uncertainty on flux represents one of the highest to deal with. The goal of this section is to find a way to measure the flux of BNB with the highest precision possible through the neutrino elastic scattering channel because of its well know cross section. A neutrino elastic scattering event has a particular signature of only a detected electron in the final state. SBND has been chosen for this measure because its position allows an almost zero neutrino-oscillation condition and a very high event rate, which means a reasonable statistic for the

12

neutrino elastic scattering channel. As shown in figure 7 the beam composition includes both neutrino and anti-neutrino of electon and muon flavour. All of them can undergo elastic scattering with an electron and all these events will just look alike inside the detector. There is no way a priori to discriminate one from another. The events generated in the simulation are reported below.

$$\nu_\mu e^- \rightarrow \nu_\mu e^- \quad \text{(371 events, 92.3\%)}$$
$$\nu_e e^- \rightarrow \nu_e e^- \quad \text{(18 events, 4.4\%)}$$
$$\overline{\nu}_\mu e^- \rightarrow \overline{\nu}_\mu e^- \quad \text{(10 events, 2.5\%)}$$
$$\overline{\nu}_e e^- \rightarrow \overline{\nu}_e e^- \quad \text{(Too low to be considered in the analysis, 0.2\%)}$$

Each elastic scattering interaction type can be correlated to the others because of the nature of the decays of the particles, such as pions and kaons, that are involved in the neutrino beam production. In this way all the elastic scattering events can be considered as signal and events can be weighted according to their cross section.

$$\sigma_{\nu_e e \rightarrow \nu_e e} = \frac{G_F^2 s}{\pi}\left[\left(\frac{1}{2}+\xi\right)^2 + \frac{1}{3}\xi^2\right] = 9.5 \cdot 10^{-49} m^2 (E_\nu/1MeV) \tag{1}$$

$$\sigma_{\overline{\nu}_e e \rightarrow \overline{\nu}_e e} = \frac{G_F^2 s}{\pi}\left[\frac{1}{3}\left(\frac{1}{2}+\xi\right)^2 + \xi^2\right] = 4.0 \cdot 10^{-49} m^2 (E_\nu/1MeV) \tag{2}$$

$$\sigma_{\nu_\mu e \rightarrow \nu_\mu e} = \frac{G_F^2 s}{\pi}\left[\left(\frac{1}{2}-\xi\right)^2 + \frac{1}{3}\xi^2\right] = 1.6 \cdot 10^{-49} m^2 (E_\nu/1MeV) \tag{3}$$

$$\sigma_{\overline{\nu}_\mu e \rightarrow \overline{\nu}_\mu e} = \frac{G_F^2 s}{\pi}\left[\frac{1}{3}\left(\frac{1}{2}-\xi\right)^2 + \xi^2\right] = 1.3 \cdot 10^{-49} m^2 (E_\nu/1MeV) \tag{4}$$

$$\xi = sin^2\theta_W \tag{5}$$

$$s = (P_\nu + P_e)^2 \simeq 2m_e E_\nu \tag{6}$$

The background for this measure involves all those events with only a detected electron in the final state. This is the case of the electron-neutrino charged-current events with 0 protons and 0 pions in the final state. With the LAr-TPC detectors there is no misidentification and events with only 0 protons and 0 pions can be selected as shown in figure 3. Anyway it is important to notice that if a proton

in the final state has less then 21 Mev kinetic energy, won't be able to travel, inside the detector, as far as the distance between two wires and so won't be reconstructed [**12**].
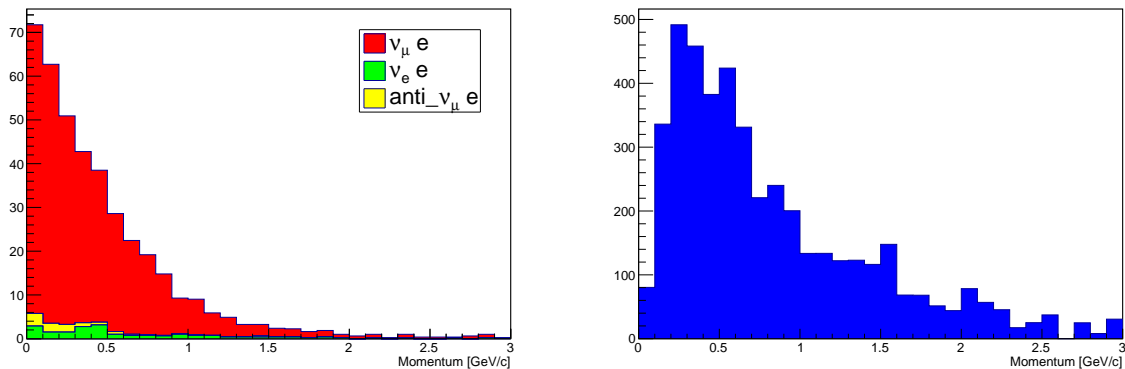
Figure 10: Electron momentum distribution for (left) elastic scattering events and (right) CC 0 π events. The behaviour looks almost the same.
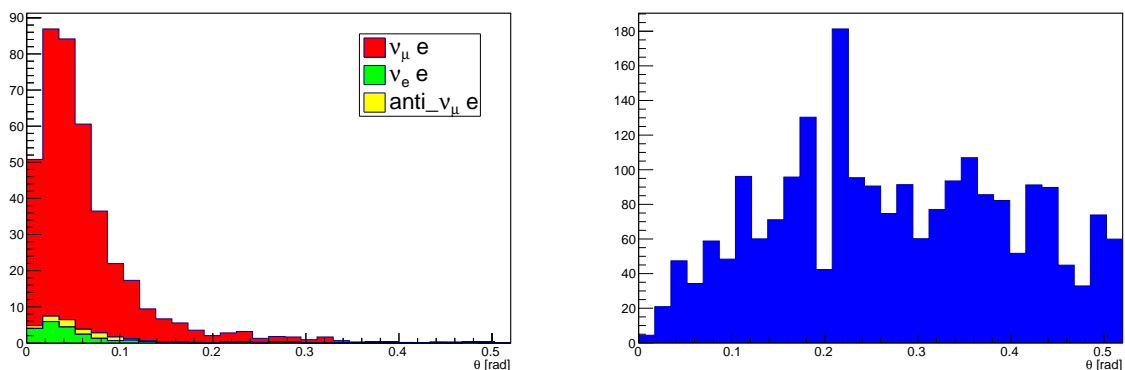
Figure 11: Electron angle distribution for (left) elastic scattering events and (right) CC 0 π events. Electrons from the elastic scattering have an angle close to 0 rad with respect to the beam direction, while for CC 0 π the outgoing angle is widers.

In the simulation almost 4500 generated events are considered as background, with a signal over background ratio of 0.09. One sort of discrimination can be done with kinematic parameters. In figure 10 and 11 are shown momentum and angle with respect to the beam direction of the outgoing electrons, both for elastic

14

scattering events and background events. From the plots is evident that, as we expected, all the elastic scattering events have the same behaviour and can't be discriminated. Separately those kinematic parameters can't be used for an efficient discrimination. They can be combined into a new variable $E\theta^2$ in order to better emphasize the particle angle behaviour which looks a more relevant signature for the signal. In figure 12 is shown the distribution for $E\theta^2$, two possible cuts can be done at 0.003 or 0.004 GeV rad^2. For these two cases the background would amount respectively to 57 and 75 events with a signal over background ratio of 7.0 and 5.3.
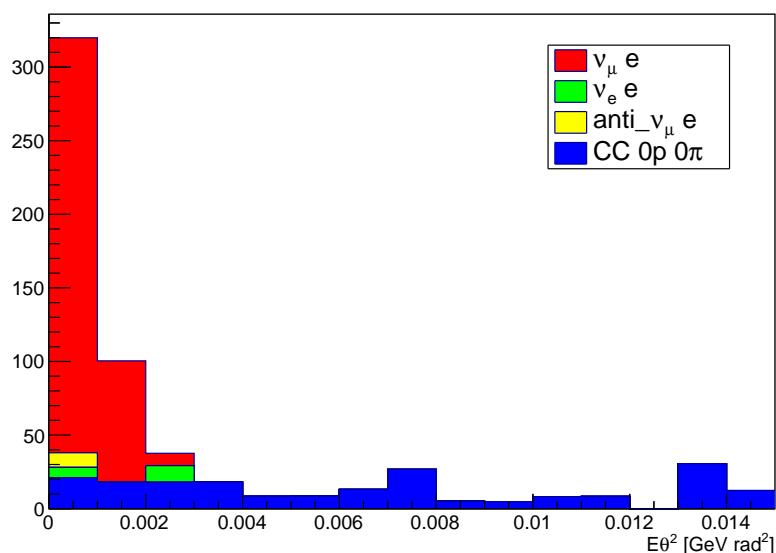
Figure 12: Distribution of the variable thought for the kinematic cut, the separation is evident.

4.2 Neutrino Charged-Current Event

Figure 13 shows that at a given initial neutrino energy multiple processes can occur. Since neutrino experiments use a nuclear target, in the BNB region, highlighted by the purple arrow, the most important neutrino-nucleus interaction channel is the CC quasi elastic scattering (QE). Nevertheless, nuclear effects play a key role in neutrino-nucleus interaction and those can lead to intra-nuclear-scattering
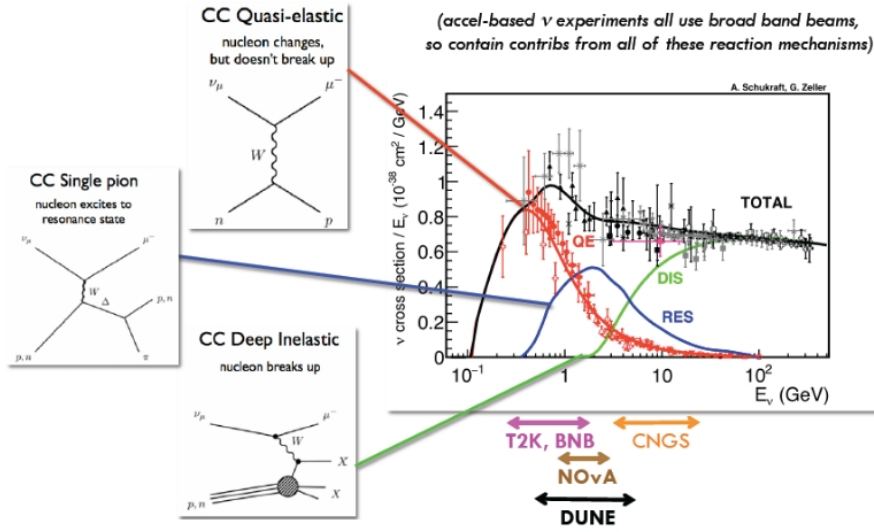
Figure 13: Neutrino CC cross section, the purple arrow represents the energy range for the BNB.

producing particles such as gammas and pions or even capturing particles such as protons, pions and neutrons that should be appear in the final state. Studying these charged-current channels is important in order to understand how these nuclear effects affect neutrino interactions cross sections and particles kinematic. In the following two sections are reported the results of kinematic analyses for CC 0 π (4.2.1) and CC 1 π (4.2.2).

4.2.1 CC 0 pion

Expectation for CC 0 π events are reported in figure 9, with LAr-TPC detectors is possible to label events according on particles multiplicity as said in (1.2). Protons and neutrons multiplicity distributions both, for ν_μ and ν_e, are shown in 14 and 15.

Kinematic distributions are done for charged leptons in the final state and for baryons too, as shown in figure 16, 17 and 18.
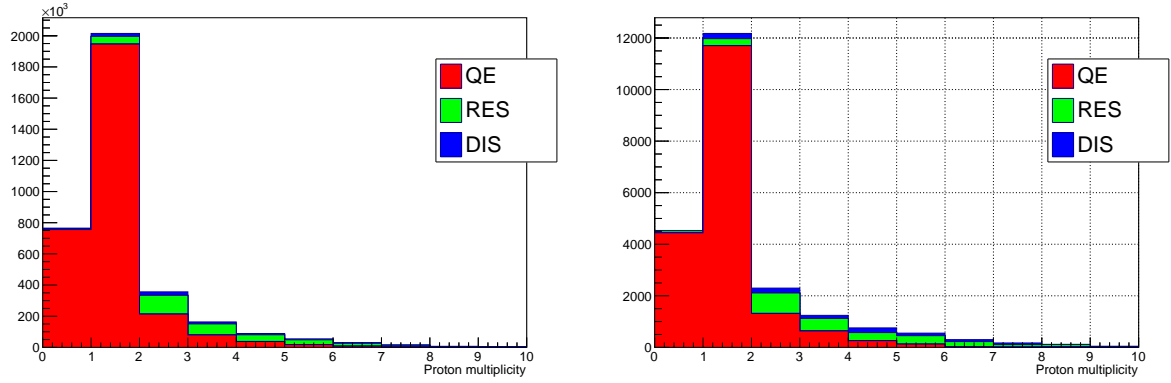
Figure 14: Proton multiplicity for (left) ν_μ CC 0π and (right) ν_e CC 0π. From truth Monte Carlo information the channel is known but due to nuclear effects resonant and deep inelastic scattering events have no pions in the final state.
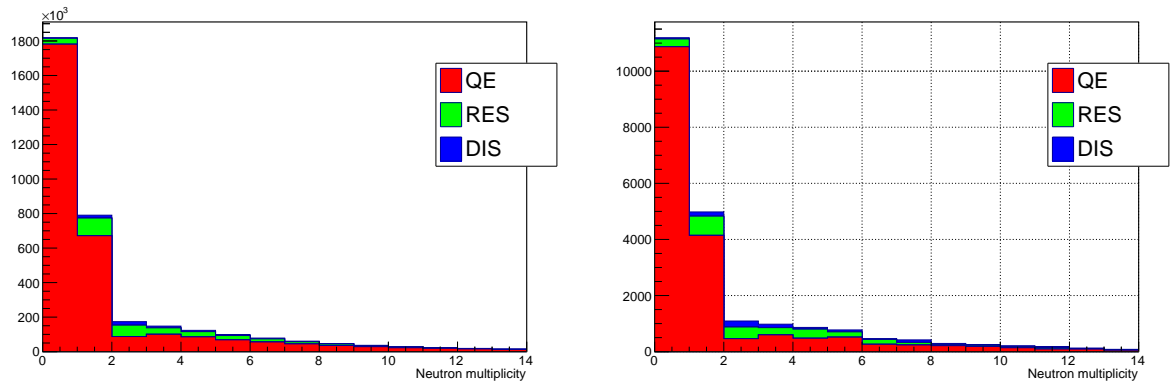
Figure 15: Neutron multiplicity for (left) ν_μ CC 0π and (right) ν_e CC 0π.
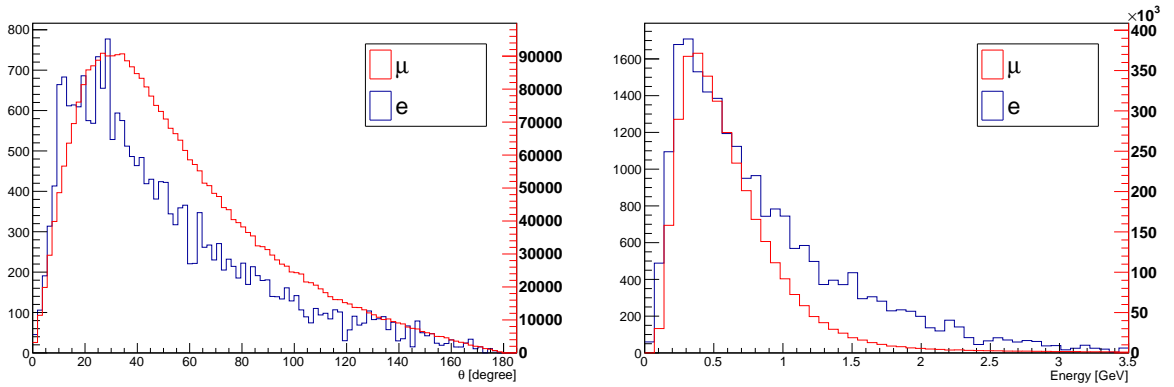
Figure 16: Left: angle distribution for charged lepton in ν_μ CC 0π (blue) and ν_e CC 0π (red). Right: energy distribution for charged lepton in ν_μ CC 0π (blue) and ν_e CC 0π (red). Distributions have different scales due to the different statistic.
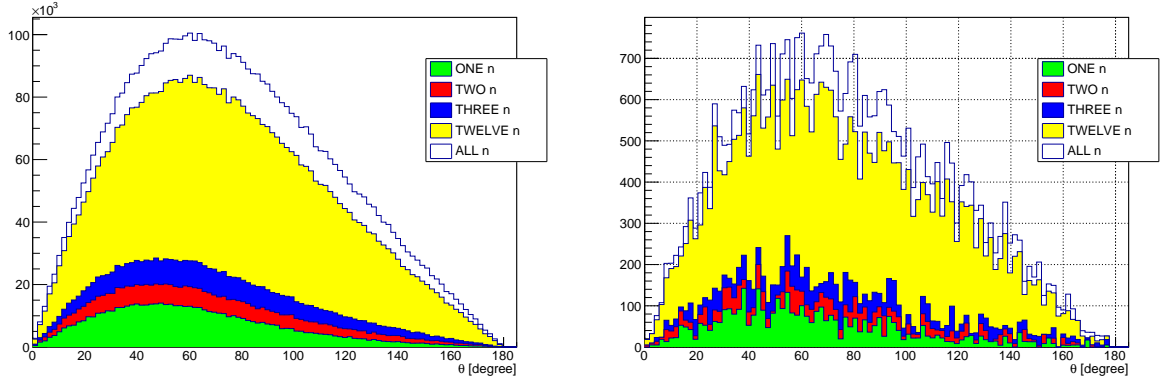
Figure 17: Left: angle distribution for neutrons in ν_μ CC 0π. Right: angle distribution for neutrons in ν_e CC 0π. More distribution are shown in order to understand how it changes considering each time more and more particles. The green distribution take into account only events with one neutron, the red one takes events with one or two neutrons and so on.
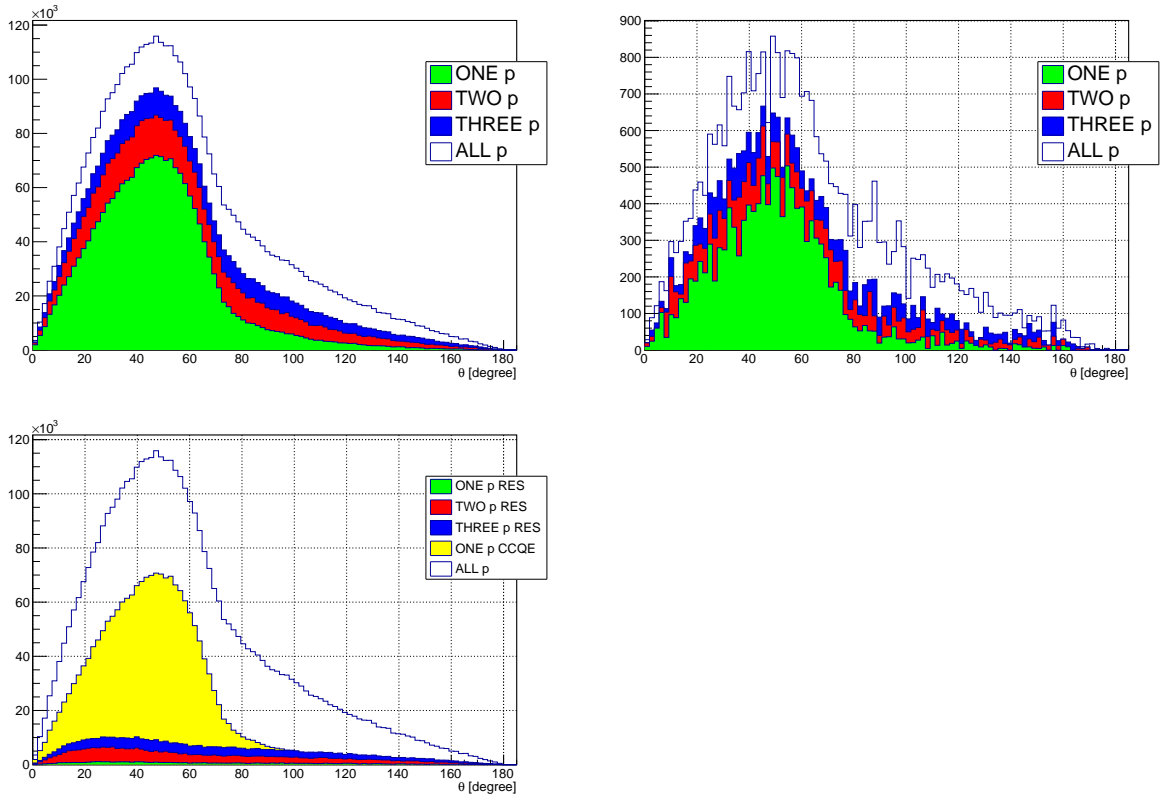
Figure 18: (Top) Left: angle distribution for protons in ν_μ CC 0π. Right: angle distribution for protons in ν_e CC 0π. More distributions are shown as for neutrons above. (Bottom) Since the angle distribution is so different from the one for neutrons more distributions, divided by CC interaction type, are shown in order to understand the angular dependence on the interaction type.

4.2.2 CC 1 pion

Expectation for CC 0 π events are reported in figure 9. Protons and neutrons multiplicity distributions both, for ν_μ and ν_e, are shown in 19 and 20. Kinematic distributions are done for charged leptons in the final state and for baryons too, as shown in figure 21, 22 and 23.
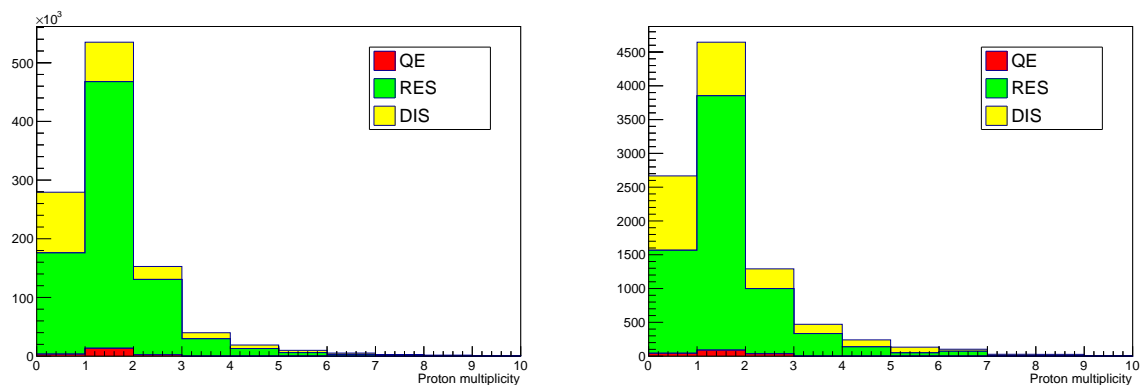
Figure 19: Proton multiplicity for (left) ν_μ CC 1π and (right) ν_e CC 1π. From truth Monte Carlo information the channel is known but due to nuclear effects even quasi elastic events have a pion in the final state.
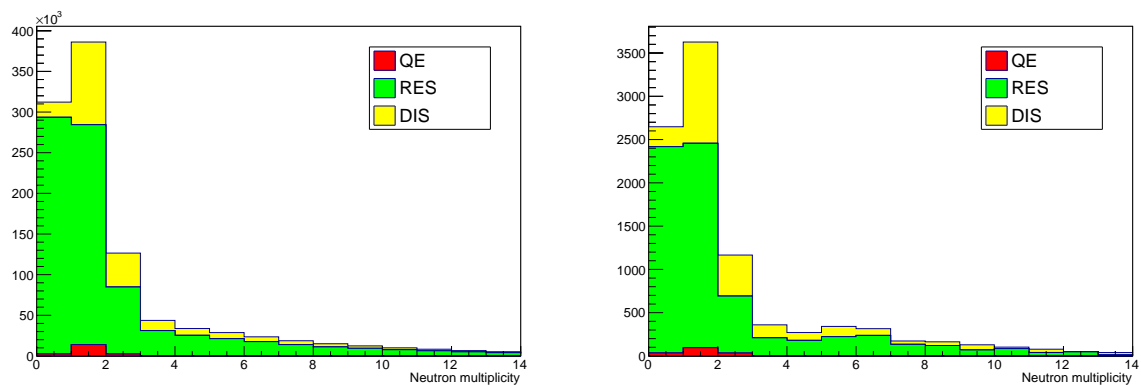
Figure 20: Neutron multiplicity for (left) ν_μ CC 1π and (right) ν_e CC 1π.
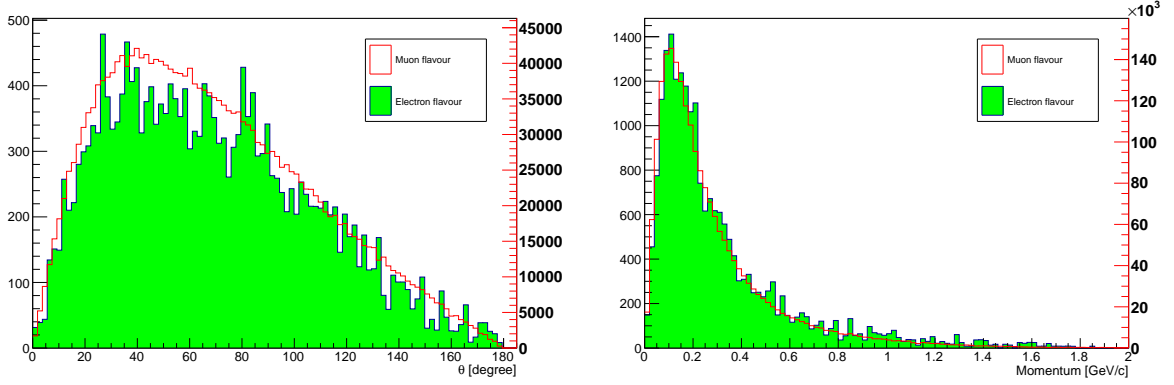
Figure 21: Left: angle distribution for neutrons in ν_μ CC 1π (red) and ν_e CC 1π (green). Right: momentum distribution for neutrons in ν_μ CC 1π (red) and ν_e CC 1π (green).Distributions have different scales due to the different statistic.
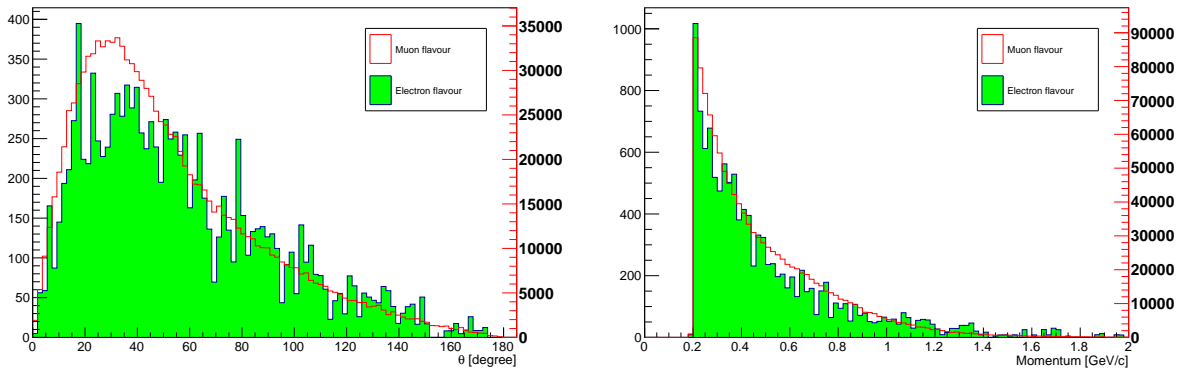
Figure 22: Left: angle distribution for protons in ν_μ CC 1π (red) and ν_e CC 1π (green). Right: momentum distribution for protons in ν_μ CC 1π (red) and ν_e CC 1π (green), the initial gap is due to the 21 MeV kinetic energy cut.

21
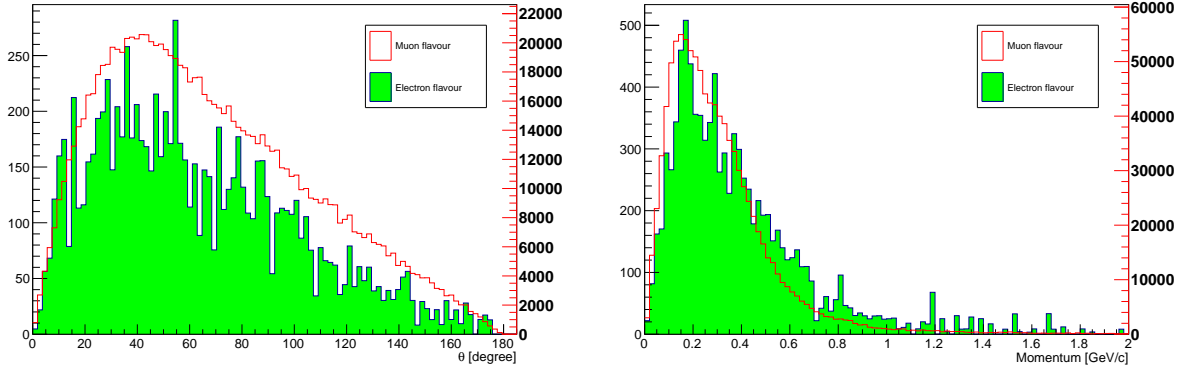
Figure 23: In CC 1π it is possile to study the kinematics for pions. Left: angle distribution for π^+ in ν_μ CC 1π (red) and ν_e CC 1π (green). Right: momentum distribution for π^+ in ν_μ CC 1π (red) and ν_e CC 1π (green).

5 Conclusion

This report explains my analysis for some neutrino-argon interactions simulated with GENIE(v2.8) for the SBND active volume. Precise neutrino-nucleus cross section measurements are a fundamental prerequisite for every neutrino oscillation experiment, including the future LAr long-baseline neutrino program. The SBND detectors will collect neutrino samples with high statistics and will make the worlds best measurements of ν_μ-Ar and ν_e-Ar scattering, including rarer processes such as ν_e-e scattering, strange particle production, multi-nucleon and multi-pion production, and coherent scattering with an argon nucleus. Working with the SBND collaboration I had the possibility to understand a lot about neutrino interactions both with electrons and nuclei.

References

1 P. Wilson et al., Program Definition Status Report: Short-Baseline Neutrino Oscillation Program on the Fermilab Booster Neutrino Beam, submitted to the Fermilab PAC in July 2014.

2 A.A. Aguilar-Arevalo et al. (MiniBooNE Collaboration), The Neutrino Flux prediction at MiniBooNE, Phys.Rev. D79, 072002 (2009), arXiv:0806.1449 [hep-ex].

3 A. A. Aguilar-Arevalo et al. (MiniBooNE Collaboration), First measurement of the muon neutrino charged current quasielastic double differential cross section, Phys. Rev. D 81, 092005 (2010).

4 MicroBooNE project, The MicroBooNE Technical Design Report, CD3b review (February 2012).

5 T. Briese, L. Bugel, J.M. Conrad, M. Fournier, C. Ignarra, et al., Testing of Cryogenic Photomultiplier Tubes for the MicroBooNE Experiment, JINST 8, T07005 (2013), arXiv:1304.0821 [physics.ins-det].

6 C. Rubbia, M. Antonello, P. Aprili, B. Baibussinov, M. Baldo Ceolin, et al., Underground operation of the ICARUS T600 LAr-TPC: first results, JINST 6, P07011 (2011), arXiv:1106.0975 [hep-ex].

7 S. Amerio et al. (ICARUS Collaboration), Design, construction and tests of the ICARUS T600 detector, Nucl.Instrum.Meth. A527, 329410 (2004).

8 A.A. Aguilar-Arevalo et al. (MiniBooNE Collaboration), A Search for electron neutrino appearance at the $\Delta m^2 \sim 1$ eV^2 scale, Phys.Rev.Lett. 98, 231801 (2007), arXiv:0704.1500 [hep-ex].

9 A.A. Aguilar-Arevalo et al. (MiniBooNE Collaboration), Unexplained Excess of Electron-Like Events From a 1-GeV Neutrino Beam, Phys.Rev.Lett. 102, 101802 (2009), arXiv:0812.2243 [hep-ex].

10 A.A. Aguilar-Arevalo et al. (MiniBooNE Collaboration), Improved Search for $\overline{\nu}_\mu \to \overline{\nu}_\mu$ Oscillations in the MiniBooNE Experiment, Phys.Rev.Lett. 110, 161801 (2013), arXiv:1207.4809 [hep-ex].

11 H. Chen et al. (MicroBooNE Collaboration), Proposal for a New Experiment Using the Booster and NuMI Neutrino Beamlines: MicroBooNE, (2007).

12 R. Acciarri et al. (ArgoNeuT Collaboration), Detection of back-to-back proton pairs in charged-current neutrino interactions with the ArgoNeuT detector in the NuMI low energy beam line, Phys. Rev. D 90, 012008 (2014).